http://dx.doi.org/10.5012/bkcs.2012.33.8.2553

Monte Carlo Simulation on Adsorption Properties of Benzene, Toluene, and *p*-Xylene in MCM-41

Sung Doo Moon

Department of Chemistry, Pukyong University, Busan 608-737, Korea. E-mail: sdmoon@pknu.ac.kr
Received March 10, 2012, Accepted May 3, 2012

The adsorption properties of benzene, toluene, *p*-xylene in MCM-41 with heterogeneous and cylindrical pore were studied using grand canonical ensemble Monte Carlo simulation. The simulated isotherms were compared with experimental ones, and the different adsorption behaviors in MCM-41 with pore diameters of 2.2 and 3.2 nm were investigated. The simulated adsorption amounts above the capillary-condensation pressure agreed with the experimental ones. The simulation results showed that most molecular planes were nearly parallel to the pore axis. This orientation was not affected by the molecular position in the pore. The molecular planes were nearly parallel to the pore surface for the adsorbate molecules close to the pore wall, and the molecules in the MCM-41 with the pore diameter of 3.2 nm were ordered along the pore axis.

Key Words : MCM-41, Monte Carlo, Benzene, Toluene, *p*-Xylene

Introduction

MCM-41 possesses a well-defined pore structure with apertures in the range of 1.5-10 nm, which can be controlled by a careful choice of surfactants, auxiliary chemicals, and reaction parameters.[1] The high surface area, regular pore shape, narrow pore size distribution, large pore volume, and tunable pore size, in conjunction with the high thermal, chemical, and mechanical stability of MCM-41 are highly conducive to numerous important applications.[2] MCM-41 materials have been widely used as adsorbents, catalysts, catalyst supports, molecular sieves, nanoreactors, molecular hosts and so forth.[3] In particular, after surface modification with organic moieties, MCM-41 becomes an excellent starting materials for creating hybrid organic-inorganic composites with potential for important applications in catalysis, separation, and nanotechnology.[4] MCM-41 has been mainly used in studies on the structural and dynamical properties of confined fluids. This is because the conventional porous materials such as glass and sintered silica have a rather wide distribution of pore size and shapes, which introduce an ambiguity in the interpretations of experimental results.[5] Grand canonical ensemble Monte Carlo (GCMC) simulation, in which the chemical potential, temperature, and volume of a system are fixed, has been used to investigate the adsorption of molecules in porous materials such as zeolite and carbon nanotubes. For instance, GCMC simulations for CH_4,[6] C_2H_6,[6,7] CO_2,[7,8] CCl_4,[9] hexane,[10] 2-methyl pentane,[10] cyclohexane[10] in MCM-41 were studied.

The aim of this study was to calculate the adsorption properties of benzene, toluene, and *p*-xylene in silanol-free MCM-41 at 298 K using GCMC simulations, in which the molecules were modeled explicitly. The following section describes the details of the MCM-41 model, molecular model, and simulation method. Thereafter, the simulation results are presented, compared with the experimental values, and discussed.

Model and Simulation Method

An MCM-41 structure with a heterogeneous surface and cylindrical pore was generated using the procedure described in previous work.[11] The pore length and wall thickness of the two simulation boxes were 3.2 and 0.95 nm, respectively. The pore diameter, *D*, was 2.2 nm for one simulation box and 3.2 nm for the other one. Figure 1 shows the geometry of the simulation box and a top view of the pore of the MCM-41 model.[11] The non-bonded interaction between the *i* site and *j* site was calculated using the coulombic and Lennard-Jones (LJ) potential:

$$u_{ij} = \frac{q_i q_j e^2}{r_{ij}} + 4\varepsilon_{ij}\left[\left(\frac{\sigma_{ij}}{r_{ij}}\right)^{12} - \left(\frac{\sigma_{ij}}{r_{ij}}\right)^{6}\right] \quad (1)$$

where r_{ij} is the distance between the *i* site and *j* site, q_i is a partial charge located at the *i* site, and *e* is the electronic charge. ε_{ij} and σ_{ij} were obtained using the standard Lorentz-

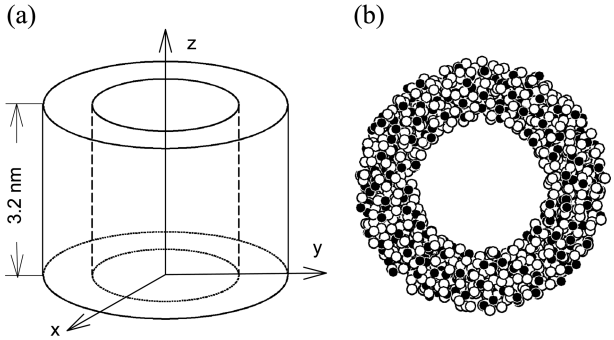

Figure 1. (a) The geometry of the simulation box of MCM-41 model. The z axis is taken along the pore axis. (b) Top view of the pore of MCM-41 model. Filled and empty circles denote silicon and oxygen atoms, respectively.

Table 1. LJ parameter for benzene, toluene, *p*-xylene, and MCM-41

site	σ (nm)	ε/k (*K*)	site	σ (nm)	ε/k (*K*)
C[a]	0.355	35.225	CH_3[b]	0.3923	72
H[a]	0.242	15.097	O[c]	0.2708	101.6
Si[d]	0	0			

[a]from ref. 14. [b]from ref. 12. [c]from ref. 8. [d]from ref. 11

Table 2. Atomic charge *q* for benzene, toluene, *p*-xylene, and MCM-41 given in units of electronic charge, *e*[a]

benzene[b]	C	–0.15	H	0.15
toluene[c]	C_α	–0.09	C_β	–0.19
	C_γ	–0.19	C_δ	–0.2
	CH_3[d]	0.1	H_β	0.19
	H_γ	0.19	H_δ	0.19
p-xylene[e]	C_α	–0.2835	C_β	–0.1161
	CH_3	0.2025	H_β	0.1566
MCM-41[f]	O	–0.18	Si	0.36

[a]see text for details. [b]from ref. 12. [c]calculated using AM1 method in ref. 15. [d]estimated value. [e]from ref. 12. [f]from ref. 8

Berthelot combining rules given by

$$\sigma_{ij} = 0.5(\sigma_i + \sigma_j) \text{ and } \varepsilon_{ij} = \sqrt{\varepsilon_i \varepsilon_j}\,. \quad (2)$$

The CH_3 moieties of the adsorbate molecule were considered to be single interaction pseudo-atoms located at the center of the carbon atoms, and the bond lengths and bond angles in the molecules were fixed in the simulation. The following bond lengths were adopted for the adsorbate molecules: r(C-C) = 0.14 nm,[12] r(C-H) = 0.1085 nm,[13] and r(CH_3-C)=0.151 nm.[12] A bond angle[13] of 120° was adopted for C-C-C, C-C-CH_3, and C-C-H. The LJ parameter and atomic charge of the sites are summarized in Table 1 and 2, respectively. C_α is the carbon atom connected to the CH_3 moiety. C_β, C_γ, and C_δ are the carbon atoms separated by one, two, and three C-C bonds in the benzene ring from C_α, respectively. H_β, H_γ, and H_δ are the hydrogen atoms connected to C_β, C_γ, and C_δ, respectively.

Simulation Method. Five types of trial moves were used for the Monte Carlo simulation in this work, as follows: (a) molecule translation, (b) molecule rotation, (c) inserting a molecule, (d) removing a molecule, and (e) regrowing a molecule. The details for the calculation of the potential and the simulation method are given in ref. 11. In this work, the simulations were performed in MC cycles. In each MC cycle, first, trial moves equal to 30 times the number of molecules in the simulation box occurred with the following probabilities: 30%, 30%, and 40% for moves (a), (b), and (e), respectively. Then, either a move (c) or move (d) was attempted. For moves (a) and (b), the maximum move was adjusted to give an average acceptance ratio of 40% every 100 MC cycles. $3 \times 10^3 \sim 2.4 \times 10^4$ MC cycles were discarded before 4×10^3 MC cycles for equilibrium were performed. The properties of the system were calculated by accumulating the adsorption properties every MC cycle and then averaging them. The initial configurations below the capillary-condensation pressure, P_c, were obtained using an NVT simulation that consisted of move (a), (b), and (e). In the NVT simulation, 2 and 3-12 molecules were used in the simulation boxes for MCM-41 with D = 2.2 and 3.2 nm, respectively. For the system above P_c, the last configuration of each run was used as the initial configuration of the next run to equilibrate faster.

Results and Discussion

Figure 2 shows the experimental and simulated adsorption isotherms of benzene, toluene, and *p*-xylene in MCM-41 with D = 3.2 and 2.2 nm, where the adsorption amounts are presented as mmole of the adsorbed molecules per cubic cm of pore volume. Here, P_0 denotes the saturated vapor pressure. In the calculation of the pore volume, the roughness and inhomogeneity of the pore wall were not considered. The pore volume was simply calculated as $\pi D^2 H/4$, where H is the pore length. The inset of Figure 2(a) shows the adsorption amounts per mass of MCM-41, which were calculated using the porosity as a conversion factor. The experimental data given by Carrott *et al.*[16] were used to

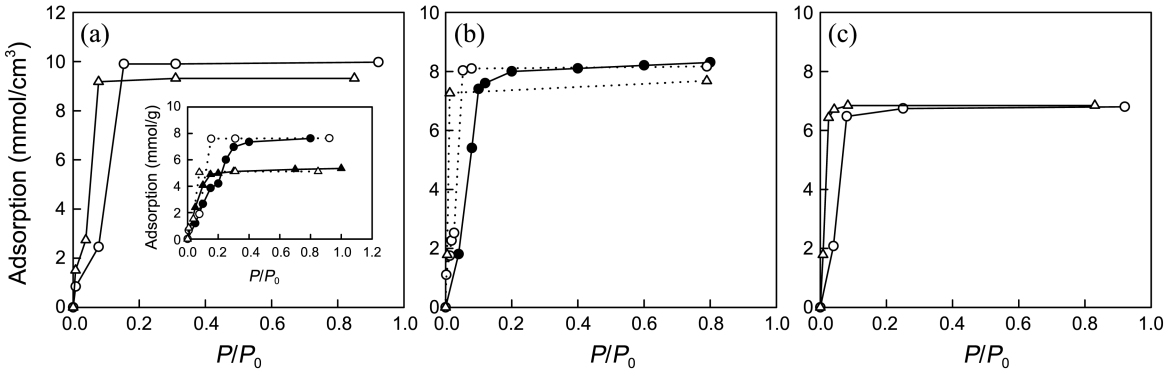

Figure 2. The experimental (filled points) and simulated (empty points) adsorption isotherms in MCM-41 with D = 3.2 (circle points) and 2.2 nm (triangle points): (a) benzene, (b) toluene, and (c) *p*-xylene. The inset in Figure 2(a) shows the adsorption amount per mass of MCM-41. Solid and dotted lines are guides for eye.

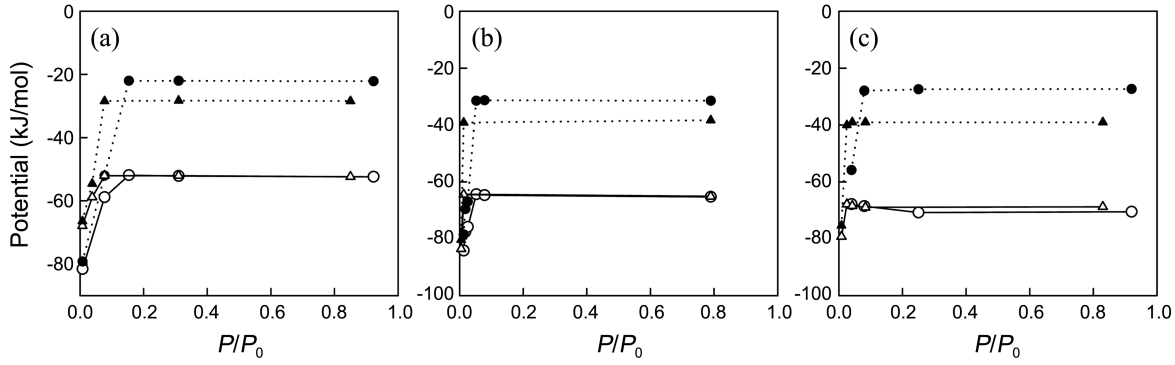

Figure 3. The total potential (empty points) and the potential of the adsorbate/adsorbent (filled points) in MCM-41 with D = 3.2 (circle points) and 2.2 nm (triangle points): (a) benzene, (b) toluene, and (c) *p*-xylene. Solid and dotted lines are guides for eye.

obtain the porosity of the MCM-41 model for the adsorption of benzene. The details for the calculation of the porosity of the MCM-41 model are given in ref. 11. The experimental data[17] in Figure 2(b) are for D = 3.3 nm, which is slightly different from the value of D used in this work. Only the simulated isotherm of *p*-xylene is plotted in Figure 2(c) because no experimental isotherm could be found for a direct comparison with the simulated one.

Figure 2 shows that the calculated isotherms are similar to type I according to the IUPAC classification, which is unusual for nanoporous adsorbents. Figure 2 shows that the capillary-condensation appears at a very low pressure, and P_c increases for a given adsorbate with an increase in D. The adsorption amounts for the benzene and toluene in MCM-41 with D = 3.2 nm is slightly larger than those with D = 2.2 nm above P_c, which probably suggests that the benzene and toluene molecules are packed less efficiently in the smaller pore. Figure 2 shows that the simulated isotherms of benzene and toluene above P_c agree with the experimental ones. However, the difference in the adsorption amounts between the simulation and experiment is noticeable at a low P/P_0. The main reason for the difference may imply that the geometry and heterogeneity of the pore wall were not sufficiently taken into account. Some researchers reported that the geometry and heterogeneity of the pore wall had a large effect on the adsorption amounts. For example, He and Seaton[7] showed that the simulated adsorption isotherms of adsorbates in MCM-41 with amorphous structure were in agreement with the experimental ones better than those in MCM-41 with homogeneous structure. Coasne *et al.*[18] showed that the adsorption amounts of argon were affected by the surface roughness of the pore wall at low pressure because of the argon atoms trapped in infractions of the pore surface. Although the MCM-41 structure possesses simply one-dimensional cylindrical pore, it is difficult to accurately reproduce the experimental isotherm using a molecular simulation because of its non-crystalline structure. In order to mimic the real MCM-41 structure, various pore sizes and/or thicknesses of pore walls can be introduced in a model of MCM-41. For example, Zhuo *et al.*[19] employed an MCM-41 structural model in which the pore radii had a Gaussian distribution based on an experimental radius. Puibasset[20] developed a large-scale porous material model with 1000 pores and a length of several micrometers, in which the heterogeneity of the pores was described by Gaussian and uniform distributions to characterize the disorder in a given pore and the disorder between the pores.

Figure 3 shows the total potential and the potential of the adsorbate/adsorbent in MCM-41 with D = 2.2 and 3.2 nm. The potential of the adsorbate/adsorbate corresponds to the difference between the total potential and the potential of the adsorbate/adsorbent. Figure 3 shows that the potential of the adsorbate/adsorbent is almost similar to the total potential at a very low P/P_0. This suggests that the molecules are adsorbed in the region close to the pore wall at a very low pressure, and that the distances between the molecules are large at a very low pressure. In addition, Figure 3 shows that the interaction between the adsorbate molecule and the adsorbent with a narrow pore is stronger than that with a large pore. Below P_c, the potential of the adsorbate/adsorbent increases with the adsorption amount. This indicates that the molecules to be adsorbed at a high P/P_0 are located farther from the pore wall than those at a low P/P_0. The isosteric heat, q_{st}, in a pore at a high P/P_0 was calculated as follows:[21]

$$q_{st} = RT - <U> - <N>\left(\frac{\partial <U>}{\partial <N>}\right)_{T,V} \quad (3)$$

where U is the potential of the adsorbate. The q_{st} values for D = 3.2 nm were 54.6, 67.3, and 72.5 kJ/mol for benzene at $P/P_0 > 0.154$, toluene at $P/P_0 > 0.053$, and *p*-xylene at $P/P_0 > 0.08$, respectively. The q_{st} values for D = 2.2 nm were 54.7, 67.3, and 71.0 kJ/mol for benzene at $P/P_0 > 0.077$, toluene at $P/P_0 > 0.013$, and *p*-xylene at $P/P_0 > 0.025$, respectively, while the heats[22] of condensation for bulk benzene, toluene, and *p*-xylene are 33.83, 38.01, and 42.4 kJ/mol, respectively.

Figures 4 and 5 show the relative densities, ρ_r, of molecules in MCM-41 with D = 2.2 and 3.2 nm as a function of the distance from the pore axis, respectively. The ρ_r of the molecules is the ratio of the density of the adsorbate molecules calculated by considering the mass-center of the molecules in the pore to that in the bulk liquid, while the ρ_r of the CH_3 moieties is the ratio of the density of the CH_3

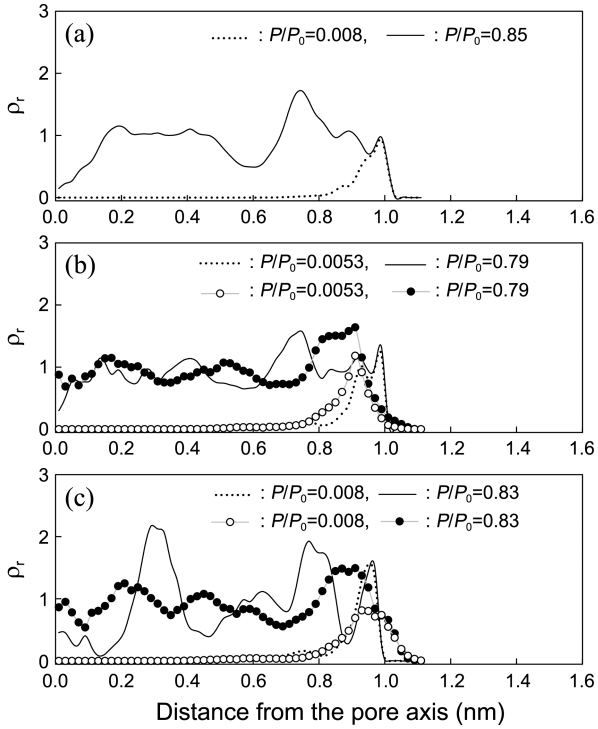

Figure 4. Relative density, ρ_r, of (a) benzene, (b) toluene, and (c) *p*-xylene in MCM-41 with D = 2.2 nm as a function of the distance from the pore axis. Solid and dotted lines are for mass-center of the molecules, while gray lines with filled and empty circles are for the CH_3 moiety of the molecules.

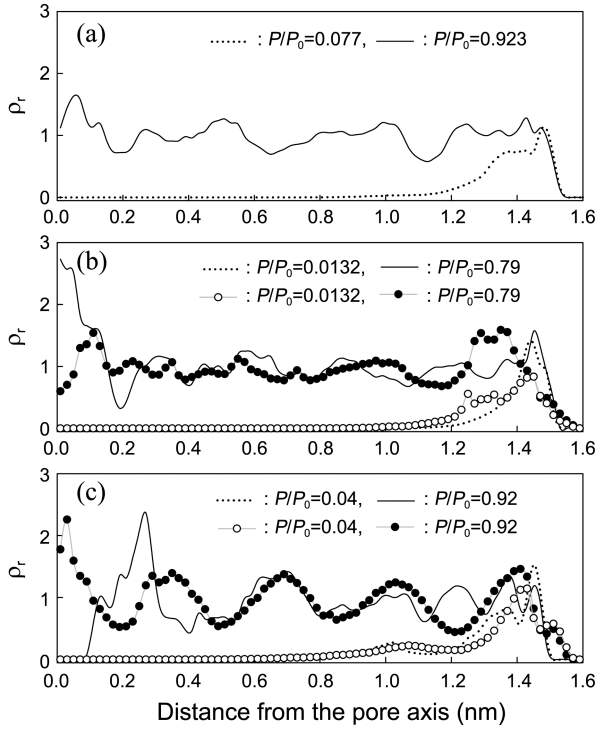

Figure 5. As in Figure 4 but for MCM-41 with D = 3.2 nm.

moieties in the pore to that in the bulk liquid. The dotted line corresponds to the ρ_r of the molecules just below P_c. In general, a multilayer of molecules in the nanopore appears after the molecules form a monolayer at a very low P/P_0, and then the molecules fill rapidly at P_c. Finally, the isotherms are nearly flat above P_c. As shown in Figures 4 and 5, the adsorption behavior of the adsorbate molecules at a low P/P_0 differs somewhat from the typical adsorption behavior mentioned above. Figures 4 and 5 show that for a given adsorbate molecule and a given D, the ρ_r peaks of the molecules located close to the pore wall just below P_c are almost similar to those above P_c, suggesting that the adsorption on adsorptive sites close to the pore wall has already been finished below P_c. A similar phenomenon for benzene adsorption in MCM-41 was reported by Coasne *et al.*[23] This phenomenon can probably be attributed to the strong interaction between the adsorbate molecule and adsorptive site. The average densities of the adsorbates in the two different pores are calculated to be 0.75, 0.72, and 0.707 g/cm^3 for benzene, toluene, and *p*-xylene, respectively (see Figure 2). These values are smaller than the corresponding liquid densities[24] by about 16%, which results from the low densities of the adsorbate molecules close to the pore wall (see Figures 4 and 5). Figures 4(b) and 5(b) show that for the toluene molecules in the layer close to the pore wall, the distances between the CH_3 moieties and pore wall are mostly larger than those between the mass-centers of the molecules and the pore wall. In contrast, the *p*-xylene molecules in the layer close to the wall have a tendency for one of the CH_3 moieties in the molecule to be located more closely to the pore wall than the mass-center of the molecule, as shown in Figures 4(c) and 5(c).

The θ, ψ, and ω angles of the adsorbate molecule within several pore regions were calculated in order to investigate the orientation of the molecules. The θ and ψ angles are defined as the angle between $\vec{A}$ and the direction of the pore radius, and the angle between $\vec{A}$ and the direction of the pore axis, respectively, where $\vec{A}$ is a vector perpendicular to the benzene ring (molecular plane) as shown in Figure 6. The ω is the angle between the pore axis and C-CH_3 bond in

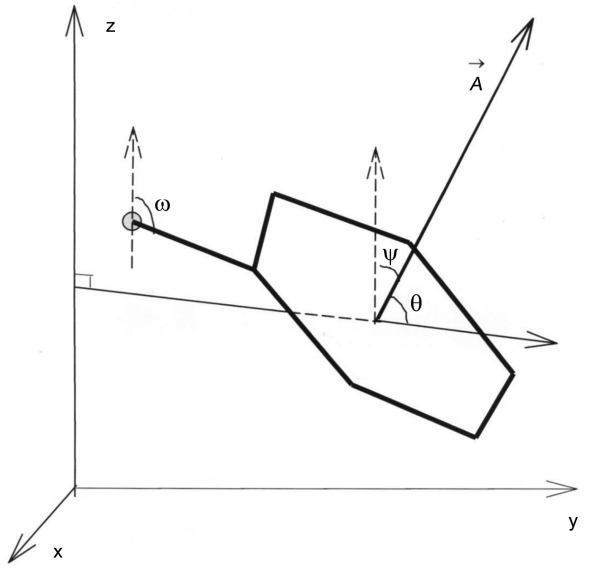

Figure 6. Definition of θ, ψ, and ω angles.

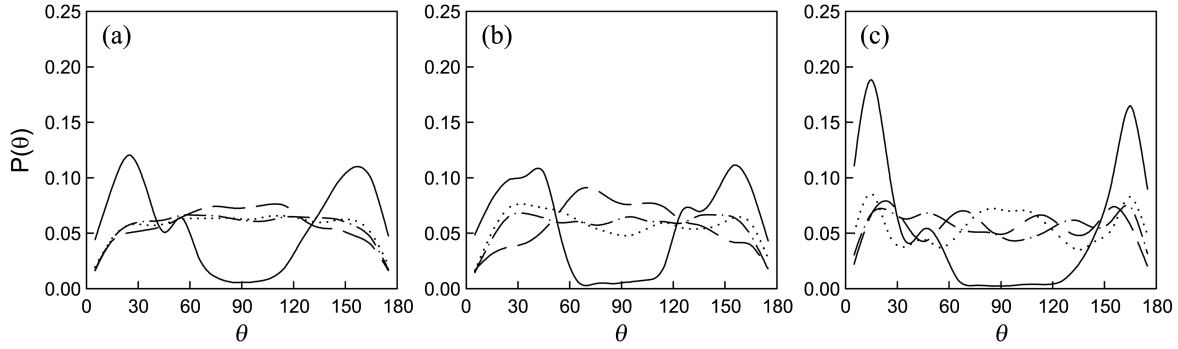

Figure 7. θ angle probabilities, $P(\theta)$, within 4 pore regions with D = 3.2 nm: (a) benzene at P/P_0 = 0.923, (b) toluene at P/P_0 = 0.79, and (c) *p*-xylene at P/P_0 = 0.92. The ranges of the first, second, third, and fourth regions are 1.3 nm ≤ x < 1.6 nm (———), 1.0 nm ≤ x < 1.3 nm (– – –), 0.5 nm ≤ x < 1.0 nm (— · — · –), and 0 ≤ x < 0.5 nm (·····), where x is the distance from the pore axis.

toluene or *p*-xylene molecules. Figure 7 shows the θ angle probabilities, $P(\theta)$, within 4 pore regions with D = 3.2 nm. The $P(\theta)$ distributions in the first regions have two large peaks near θ = 30° and 150°, indicating that the benzene, toluene, and *p*-xylene molecules near the pore wall mainly orientate their benzene rings toward the pore wall at a slightly tilted angle. In addition, Figure 7 shows that the $P(\theta)$ distributions, everywhere except in the first region, are similar to each other regardless of the θ angle and the kind of adsorbates. This means that there is a preferential orientation for the θ angle within only the region near the pore wall. Alba-Simionesco *et al.*[25] reported that most of the benzene molecules close to the pore wall tended to orientate their benzene rings parallel to the pore wall, which nearly agrees with the result in this work. Figure 8 shows ψ angle probabilities, $P(\psi)$, within 4 pore regions with D = 3.2 nm. Figure 8 shows that each of the $P(\psi)$ distributions has only one large peaks near ψ = 90°, and that the shapes of these peaks are similar to each other, indicating that most of the molecules hold their benzene rings parallel to the pore axis. This orientation is nearly independent from the kind of adsorbate and position of the molecule in the pore. In addition, the $P(\theta)$ and $P(\psi)$ distributions within 3 pore regions with D = 2.2 nm were calculated. In these calculations, the distance ranges of the 3 regions were set to 0.8 nm ≤ x < 1.2 nm, 0.4 nm ≤ x < 0.8 nm, and 0 ≤ x < 0.4 nm, where x is the distance from the pore axis. The results were similar to those for D = 3.2 nm. That is, most of the adsorbate molecules close to the pore wall tended to orientate their benzene rings parallel to the pore wall, and most of the molecules tended to have their benzene rings parallel to the pore axis regardless of their position in the pore. Thus, the $P(\theta)$ and $P(\psi)$ distributions for D = 2.2 nm are not presented for brevity.

The ρ_r of the molecules in MCM-41 as a function of the distance along the pore axis is plotted in Figure 9, which shows the ordering phenomenon of the molecules. The molecules in MCM-41 with D = 3.2 nm are more ordered than those with D = 2.2 nm. The distances between the layers are 0.54, 0.54, and 0.8 nm for benzene, toluene, and *p*-xylene, respectively, in the pore with D = 3.2 nm. The distances between the layers of the adsorbate molecules are not constant for D = 2.2 nm. According to the previous work,[11] when the neopentane and cyclohexane were adsorbed in MCM-41 at a high P/P_0, the strong adsorption layers with a regular spacing formed along the radius of pore, but not formed along the pore axis. Interestingly, these phenomena are in contrast with the adsorption phenomena of the benzene, toluene, and *p*-xylene in this work, suggesting that the molecular shape significantly affects the spatial arrangement of the adsorbate molecules. It seems that spherical or spheroidal molecules form the well-defined layers along the radius of pore in MCM-41.

In order to investigate the orientation of the *p*-xylene molecules, the ρ_r values of the CH_3 moieties of the *p*-xylene molecules in the pores with D = 3.2 and 2.2 nm are plotted as a function of the distance along the pore axis in Figures 9(c) and 9(d), respectively. The ρ_r values of the CH_3

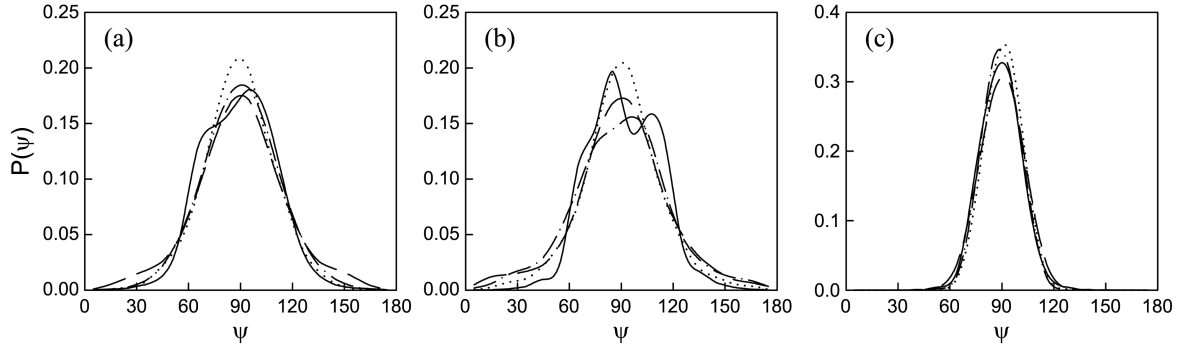

Figure 8. As in Figure 7 but for ψ angle probabilities, $P(\psi)$.

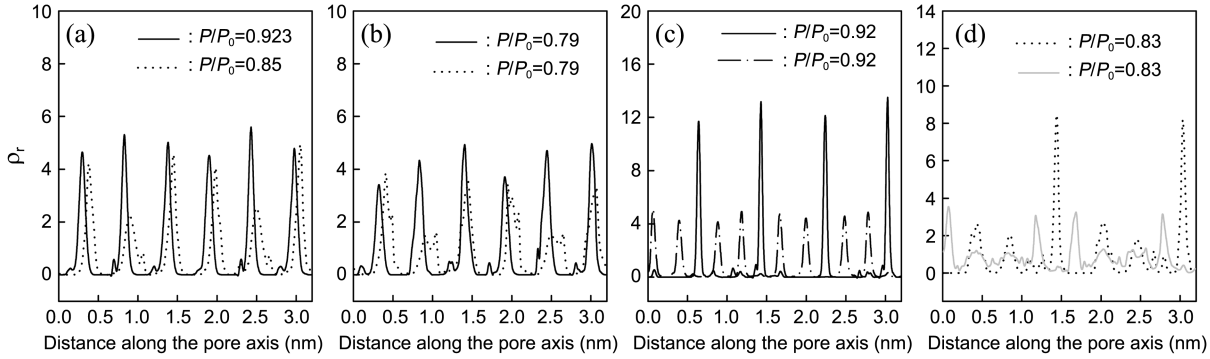

Figure 9. Relative density, ρ_r, of (a) benzene, (b) toluene, and (c, d) *p*-xylene as a function of the distance along the pore axis. Solid and dotted lines are for mass-center of the molecules in pores with D = 3.2 and 2.2 nm, respectively. Dashed-dotted and gray lines are for the CH_3 moiety of *p*-xylene molecule in pores with D = 3.2 and 2.2 nm, respectively.

moieties of the toluene molecules are not presented in Figure 9 because of complication of their peaks. Figure 9(c) shows that two ρ_r peaks for the CH_3 moieties regularly appear at distances of 0.24 nm on both sides of each of the ρ_r peaks of the molecules. This distance (0.24 nm) corresponds to the perpendicular distance between the CH_3 moiety and the layer containing the CH_3 moiety, while the distance between the CH_3 moiety and mass-center of *p*-xylene is 0.291 nm. From these two distances, the angle between the pore axis and CH_3-C bond of the *p*-xylene molecule (that is, the ω angle) can be calculated to be 34° or 146°. Figure 9(c) shows that the ρ_r peaks of the CH_3 moieties are sharp and do not overlap the ρ_r peaks of the molecules at all, indicating that the *p*-xylene molecules in the pore with D = 3.2 nm never have an orientation with $\omega \approx 90^o$.

The ρ_r peak of the molecules at 1.42 nm and the ρ_r peaks of the CH_3 moieties at 1.18 and 1.66 nm in Figure 9(d) suggest that the *p*-xylene molecules in the layer at 1.42 nm have the same orientation as in the pore with D = 3.2 nm. Again, the ρ_r peak of the molecules at 3.03 nm and the ρ_r peaks of the CH_3 moieties at 0.07 and 2.79 nm in Figure 9(d) suggest that the *p*-xylene molecules in the layer at 3.03 nm have the same orientation as in the pore with D = 3.2 nm. However, the other ρ_r peaks of the molecules and CH_3 moieties in Figure 9(d) are more difficult to interpret. Therefore, in order to further analyze the orientation of the molecules, the ω angle probabilities, $P(\omega)$, are plotted in Figure 10. Figure 10(a) shows that the $P(\omega)$ distribution of toluene in the pore with D = 2.2 nm is similar to that in the pore with D = 3.2 nm. Whereas, the $P(\omega)$ distribution of *p*-xylene for D = 2.2 nm is very different from that for D = 3.2 nm as shown in Figure 10(b). This suggests that the influence of the pore size on the $P(\omega)$ distribution increases with the size of the adsorbate molecule. Figure 10(b) shows that most of the *p*-xylene molecules in the pore with D = 3.2 nm have an orientation with ω = 34° or 146°, and that there are no molecules with orientations where ω = 60°-120°. This is consistent with the results estimated in Figure 9(c). Figure 10(b) shows that for the *p*-xylene in the pore with D = 2.2 nm, three broad peaks appear at ω = 34°, 90°, and 146°. These three peaks have similar heights, in which the peaks at

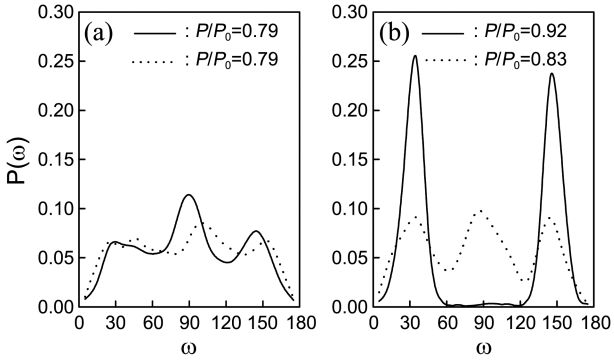

Figure 10. ω angle probabilities, $P(\omega)$, of (a) toluene, and (b) *p*-xylene in the pores with D = 3.2 (solid line) and 2.2 nm (dotted line).

ω = 34° and 146° correspond to the ρ_r peaks of the molecules at 1.42 and 3.03 nm in Figure 9(d), indicating that the *p*-xylene molecules in the layers at 1.42 and 3.03 nm in the pore with D = 2.2 nm have mainly orientations with ω = 34° or 146°. Again, the peak of ω = 90° in Figure 10(b) corresponds to the ρ_r peaks of the molecules at 0.45, 0.85, 2.05, and 2.5 nm in Figure 9(d), which overlap the ρ_r peaks of the CH_3 moieties, indicating that the *p*-xylene molecules in the layers at 0.45, 0.85, 2.05, and 2.5 nm in the pore with D = 2.2 nm have mainly orientations with ω = 90°.

Conclusion

GCMC simulations were performed to study the adsorption properties of benzene, toluene, and *p*-xylene in sinanol-free MCM-41 with D = 2.2 and 3.2 nm. The interactions between the sites were calculated using the coulombic and LJ potential. The adsorption isotherm, average potential of the adsorbate, isosteric heat of adsorption, and density of the molecules in MCM-41 were calculated. The simulated adsorption amounts for benzene and toluene above P_c agreed well with the experimental values. On the other hand, the average densities of the adsorbates in the two different pores were smaller than the corresponding liquid densities by about 16%, which accounted for the low densities of the adsorbate molecules close to the pore wall.

The orientations of the adsorbate molecules within several pore regions were calculated. The benzene, toluene, and *p*-xylene molecules near the pore wall mainly orientated their benzene rings toward the pore wall at a slightly tilted angle. In addition, most of the molecules tended to have their benzene rings parallel to the pore axis regardless of their position in the pore. On the other hand, the adsorbate molecules were ordered along the pore axis in the pore with D = 3.2 nm. The simulation results showed that for most of the *p*-xylene molecules in the pore with D = 3.2 nm, the angle between the pore axis and CH_3-C bond was 34° or 146°.

Acknowledgments. This work was supported by the Pukyong National University Research Fund in 2011 (PK-2011-40).

References

1. Zhao, X. S.; Lu, G. Q.; Millar, G. J. *Ind. Eng. Chem. Res.* **1996**, *35*, 2075.
2. Selvam, P.; Bhatia, S. K.; Sonwane, C. G. *Ind. Eng. Chem. Res.* **2001**, *40*, 3237.
3. Bhattacharyya, S.; Lelong, G.; Saboungi, M.-L. *J. Exp. Nanosci.* **2006**, *1*, 375.
4. Marschall, R.; Tolle, P.; Cavalcanti, W. L.; Wilhelm, M.; Kohler, C.; Frauenheim, T.; Wark, M. *J. Phys. Chem. C* **2009**, *113*, 19218.
5. Takahara, S.; Sumiyama, N.; Kittaka, S.; Yamaguchi, T.; Bellissent-Funel, M.-C. *J. Phys. Chem. B* **2005**, *109*, 11231.
6. Yun, J.-H.; Duren, T.; Keil, F. J.; Seaton, N. A. *Langmuir* **2002**, *18*, 2693.
7. He, Y.; Seaton, N. A. *Langmuir* **2003**, *19*, 10132.
8. Koh, C. A.; Montanari, T.; Nooney, R. I.; Tahir, S. F.; Westacott, R. E. *Langmuir* **1999**, *15*, 6043.
9. Cao, D.; Shen, Z.; Chen, J.; Zhang, X. *Microporous and Mesoporous Mater.* **2004**, *67*, 159.
10. Fox, J. P.; Bates, S. P. *Langmuir* **2005**, *21*, 4746.
11. Moon, S. D.; Choi, D. W. *Korean J. Chem. Eng.* **2009**, *26*, 1098.
12. Snurr, R. Q.; Bell, A. T.; Theodorou, D. N. *J. Phys. Chem.* **1993**, *97*, 13742.
13. Rungsirisakun, R.; Nanok, T.; Probst, M.; Limtrakul, J. *J. Mol. Graph. Model.* **2006**, *24*, 373.
14. Contreras-Camacho, R. O.; Ungerer, P.; Boutin, A.; Mackie, A. D. *J. Phys. Chem. B* **2004**, *108*, 14109.
15. MOPAC (ChemBio3D Ultra ver. 11.0); CambridgeSoft: Cambridge, MA, 2008.
16. Carrott, M. M. L. R.; Candeias, A. J. E.; Carrott, P. J. M.; Ravikovitch, P. I.; Neimark, A. V.; Sequeira, A. D. *Microporous and Mesoporous Mater.* **2001**, *47*, 323.
17. Ravikovitch, P. I.; Vishnyakov, A.; Neimark, A. V.; Carrott, M. M. L. R.; Russo, P. A.; Carrott, P. J. *Langmuir* **2006**, *22*, 513.
18. Coasne, B.; Pellenq, R. J.-M. *J. Chem. Phys*. **2004**, *120*, 2913.
19. Zhuo, S.; Huang, Y.; Hu, J.; Liu, H.; Hu, Y.; Jiang, J. *J. Phys. Chem. C* **2008**, *112*, 11295.
20. Puibasset, J. *Langmuir* **2009**, *25*, 903.
21. Gupta, A.; Clark, L. A.; Snurr, R. Q. *Langmuir* **2000**, *16*, 3910.
22. Lide, D. R. *CRC Handbook of Chemistry and Physics*; CRC Press: Boca Raton, 1999.
23. Coasne, B.; Alba-Simionesco, C.; Audonnet, F.; Dosseh, G.; Gubbins, K. E. *Langmuir* **2009**, *25*, 10648.
24. Lide, D. R.; Kehiaian, H. V. *CRC Handbook of Thermophysical and Thermochemical Data*; CRC Press: Boca Raton, 1994.
25. Alba-Simionesco, C.; Dosseh, G.; Dumont, E.; Frick, B.; Geil, B.; Morineau, D.; Teboul, V.; Xia, Y. *Eur. Phys. J. E.* **2003**, *12*, 19.